Heterogeneous Integration of InGaAs Nanowires on the Rear Surface of Si Solar Cells for Efficiency Enhancement
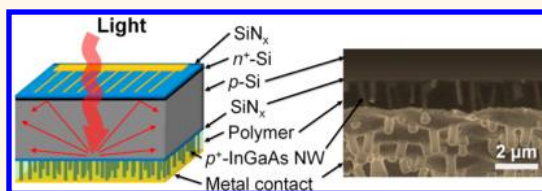
Jae Cheol Shin,[†,‡] Parsian K. Mohseni,[†] Ki Jun Yu,[†] Stephanie Tomasulo,[§] Kyle H. Montgomery,[⊥] Minjoo L. Lee,[§] John A. Rogers,[¶] and Xiuling Li[†,*]

[†]Department of Electrical and Computer Engineering and [¶]Department of Materials Science and Engineering, University of Illinois, Urbana, Illinois 61801, United States, [‡]Photonics-Energy Center, Korea Photonics Technology Institute, 500-779, Korea, [§]Department of Electrical Engineering, Yale University, New Haven, Connecticut 06520, United States, and [⊥]Department of Electrical and Computer Engineering, Purdue University, West Lafayette, Indiana 47909, United States

ABSTRACT We demonstrate energy-conversion-efficiency (η) enhancement of silicon (Si) solar cells by the heterogeneous integration of an $In_xGa_{1-x}As$ nanowire (NW) array on the rear surface. The NWs are grown *via* a catalyst-free, self-assembled method on Si(111) substrates using metalorganic chemical vapor deposition (MOCVD). Heavily p-doped $In_xGa_{1-x}As$ ($x \approx 0.7$) NW arrays are utilized as not only back-reflectors but also low bandgap rear-point-contacts of the Si solar cells. External quantum efficiency of the hybrid $In_xGa_{1-x}As$ NW-Si solar cell is increased over the entire solar response wavelength range; and η is enhanced by 36% in comparison to Si solar cells processed under the same condition without the NWs.

Silicon (Si) is of great interest for photovoltaic applications because of its natural abundance, absorption spectrum compatibility with the AM 1.5 solar spectrum, and maturity in fabrication at the commercial-scale. Various high-aspect-ratio structures such as nanowires (NWs) have been fabricated on Si surfaces to enhance the performance of solar cells. For example, NWs composed of core−shell structures are advantageous for the collection of photogenerated carriers as the shell dimensions can be tailored to be on the order of the minority carrier diffusion lengths.[1] Moreover, NW arrays on Si surfaces dramatically enhance light absorption of the solar spectrum, and thereby increase the energy-conversion-efficiency (η) of solar cells while reducing material consumption in the active-region.[2−4] Metal-assisted chemical etching (MacEtch) or reactive-ion-etching (RIE) techniques are often used to form NW arrays on Si surfaces.[3,4] However, the increase of surface area resulting from high-aspect-ratio structures leads to a dramatic increase in surface recombination, which often surpasses the advantage of superior light absorption and carrier-collection efficiency, otherwise

offered by NW arrays.[3−5] Additionally, the resulting etched surfaces are often roughened, which increases the surface recombination velocity further.[6]

The growth of catalyst-free, self-assembled $In_xGa_{1-x}As$ NW array over almost the entire composition range has been recently demonstrated by metalorganic chemical vapor deposition (MOCVD) on Si substrates.[7] The heterogeneous interface between $In_xGa_{1-x}As$ NW and Si is abrupt and the bandgap and doping of the NWs can be controlled through growth parameters. Furthermore, MOCVD grown NWs have smooth sidewalls terminated with low-index crystal planes, as opposed to the roughened sidewalls generated *via* dry etching methods.[8] In this letter, we report on the fabrication and characterization of a solar cell geometry with $In_xGa_{1-x}As$ NW arrays integrated on the back surface of a p−n junction Si cell. We show that a heavily p-doped NW array increases light absorption of the Si cell, by serving as a back-reflector, and simultaneously reduces recombination loss of the device, by acting as the rear-point-contact. The integrated heterogeneous $In_xGa_{1-x}As$ NW−Si solar cells show a significant

increase of external quantum efficiency and total energy conversion efficiency compared to planar Si solar cells with thermally diffused contact layers on both sides.

RESULTS AND DISCUSSION

Shown in Figure 1 are SEM images of $In_xGa_{1-x}As$ NW arrays grown on a Si (111) substrate *via* the catalyst-free mismatch-strain driven self-assembled mechanism by MOCVD. Prior to growth, a p-type Si (111) wafer ($\rho = 0.15-0.25$ Ω-cm) was dipped in buffered-hydrofluoric acid (BHF) for 10 min to remove the native oxide on the surface. Then, the wafer was rinsed with deionized water for 1 s, dried with nitrogen and immediately loaded into the reactor. The reactor was heated to 570 °C under 15 L/min of hydrogen carrier gas. After the temperature was stabilized, trimethylindium [$(CH_3)_3In$, TMIn], trimethylgallium [$(CH_3)_3Ga$, TMGa], and arsine (AsH_3) were simultaneously flown into the reactor. The detailed molar flow of the metalorganic sources and hydride gas can be found in Experimental Procedures. The $In_xGa_{1-x}As$ NWs are vertically oriented and heterogeneously integrated on Si. Its bandgap
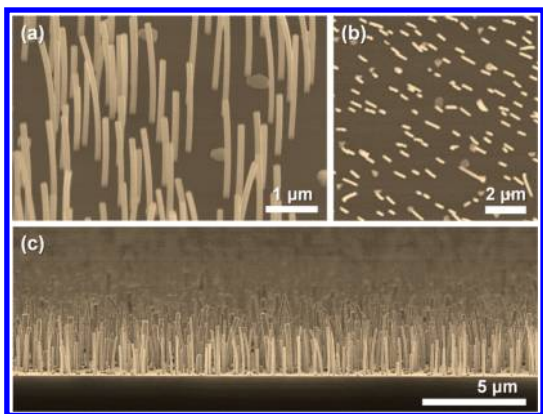
energy can be engineered by changing the indium composition.[7,9] Based on transmission electron microscopy (TEM) analysis, no misfit dislocations are found in the NWs. Details of the NW growth mechanism and structural properties can be found elsewhere.[7,9] The NWs used in this study are 2−3 μm tall, but exhibit slight bending with increasing NW lengths (Figure 1a,c). This bending effect was previously attributed to local compositional inhomogeneity, which generates nonuniform strain across the NWs.[7] The indium composition in the NW is ∼0.7 based on the photoluminescence measurement with a peak of energy at ∼0.6 eV.[7]

The number density of the NWs is ∼1.4 × 10^8/cm^2, calculated from a typical top-view SEM image taken over an area of 10 × 10 μm^2 (Figure 1b). With an average diameter of 104 nm, the NW array occupies only ∼1.5% of the Si surface area. Despite the low areal coverage, $In_xGa_{1-x}As$ NW array on Si has been shown to decrease the reflectance of light in the wavelength range of 500 nm −1 μm to below 10%, which is even lower than that of the conventional anti-reflection coating (ARC, *i.e.* SiN_x)[7] but comparable to the textured pattern or ordered nanopillar array structures.[10,11] We note that the catalyst-free self-assembled NW array formation process is simple and economical, with a total growth time of around 1 h from wafer loading to unloading, and the total consumption of the metalorganic sources and hydride gas for the growth of around 0.01 and 1 g, respectively.

Shown in Figure 2 a,b are the transmittance spectra measured from the Si sample with the $In_xGa_{1-x}As$ NW ($x \approx 0.7$) array on the back surface along with the reference Si sample, with the detector placed directly underneath and using the integrated sphere, respectively. It can be seen that wavelengths below ∼950 nm are fully absorbed for both samples because the absorption coefficient of Si is high in this range (*i.e.*, > 1 × 10^2 cm^{-1}). Above ∼950 nm, the transmittance through the bare Si reference sample gradually increases because the absorption coefficient of Si rapidly decreases near its bandgap energy.[12] By adding
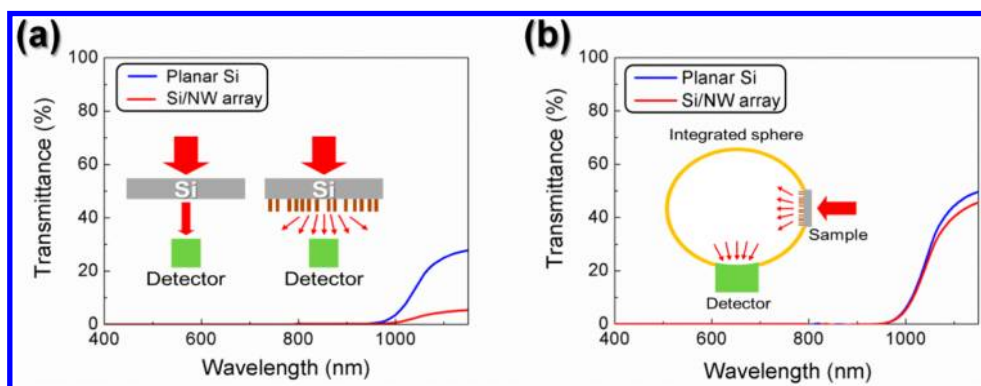

Figure 1. $In_xGa_{1-x}As$ NW array grown on a Si (111) substrate: (a) 45° tilted SEM image of vertically oriented NWs; (b) top-view SEM image over a 10 × 10 μm^2 area with a number density of ∼1.4 × 10^8/cm^2; and (c) panoramic view of a cross-section SEM image of the NWs with a height of *ca.* 2−3 μm.

Figure 2. Transmittance spectra of a Si wafer with $In_xGa_{1-x}As$ NW array on the back surface along with a bare Si reference sample, with the measurement geometry as illustrated.

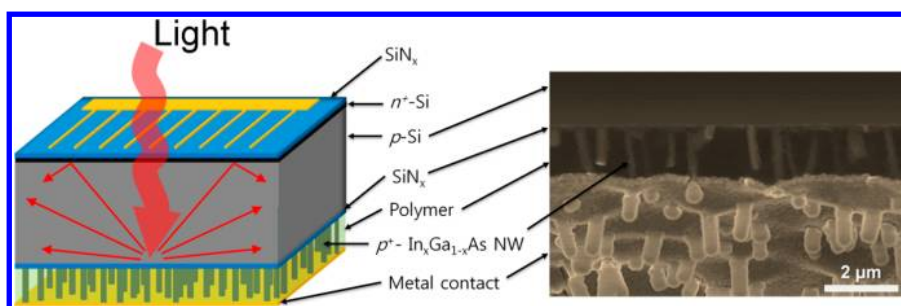**Figure 3.** Schematic illustration and the corresponding cross-sectional SEM image of a Si solar cell with an $In_xGa_{1-x}As$ NW array integrated.

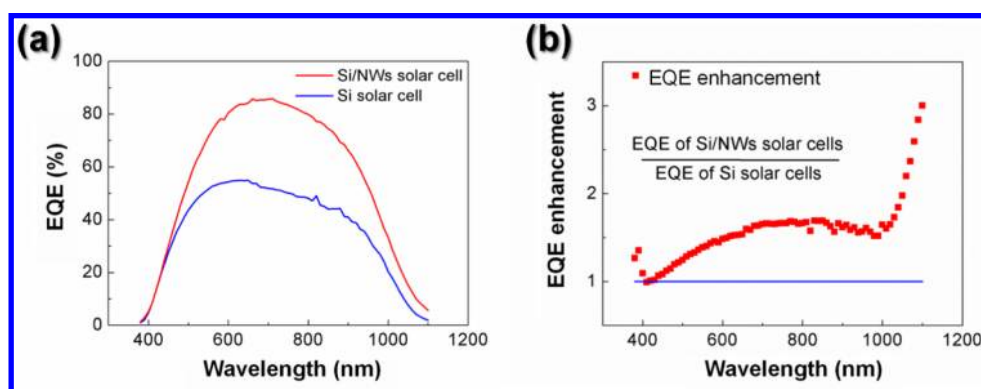**Figure 4.** EQE spectra (a) taken from the Si solar cell with $In_xGa_{1-x}As$ NW array integrated on the back surface, along with the reference Si solar cell; (b) normalized to the reference Si cell.

the $In_xGa_{1-x}As$ ($x \approx 0.7$) NW array on the backside of Si, the transmittance decreases to below 6% from ∼30% (Figure 2a). However, when an integrated sphere was used to collect the transmitted light (Figure 2b), the difference with and without the NWs is only 2−3%. This indicates that the transmitted light is scattered by the NWs into large angles (see illustrations in Figure 2 inset) so that a significant portion of the light can then be reflected into Si, recycled, and reabsorbed. The finding suggests the possibility of using the NW array as a back-reflector to enhance light absorption, similar to the role of textured back reflectors reported previously.[13−16] In particular, the use of textured photonic crystal by combining 1-D DBRs with 1-D textured grating structures led to the creation of a photonic bandgap with high reflectivity across broad spectral range.[13] Also, the use of quasi-periodic or random micro/nanopatterns led to omnidirectional low reflectivity at the semiconductor/air interface in improving the light extraction in light-emitting diodes (LEDs).[17−19] Further studies are needed to confirm the back reflector functionality of the NW arrays. Note that although the bandgap (∼0.6 eV) of $In_xGa_{1-x}As$ NWs is smaller than that of the Si, the total volume of the NW array is only ∼0.03% of the Si so absorption by the NWs should not play a significant role.

Figure 3 shows the schematic illustration and corresponding cross-sectional SEM image of an Si solar cell with the $In_xGa_{1-x}As$ NW array integrated on the back surface (Si/NWs). A SiN_x layer is deposited on the top surface of the Si cell as an ARC layer. Conventional metal Ti/Au is coated on the entire back surface for electrical contacts. In contrast, if the NWs were to be incorporated on the front surface, transparent metal contact (e.g., indium tin oxide) would have to be used to allow light to come through. However, transparent metal is generally more resistive than conventional metals, leading to significant reduction of efficiency. As illustrated in Figure 3, we believe the scattered light by the NWs is reflected to random directions by the rear surface metal to increase the optical path. Because the refractive index of SiN_x (∼2.0) is much lower than that of Si (>3.5), a considerable fraction of the reflected light reaching the top surface with an angle larger than the critical angle (i.e., $\theta_c \approx$ arcsin (n_2/n_1)) for internal reflection is reflected again toward the back surface, which increases the light absorption.[20]

In addition, the heavily doped NW array serves as a rear-point-contact.[21] It is known that many of the minority carriers are lost near the metal contact because of surface states, and the heavily doped region enhances Shockley−Read−Hall and Auger recombination. For this reason, in commercial Si solar cells, only part of the rear side is heavily p^+ doped and contacted with metal to increase collection efficiency.[21] The rest of the rear surface area is
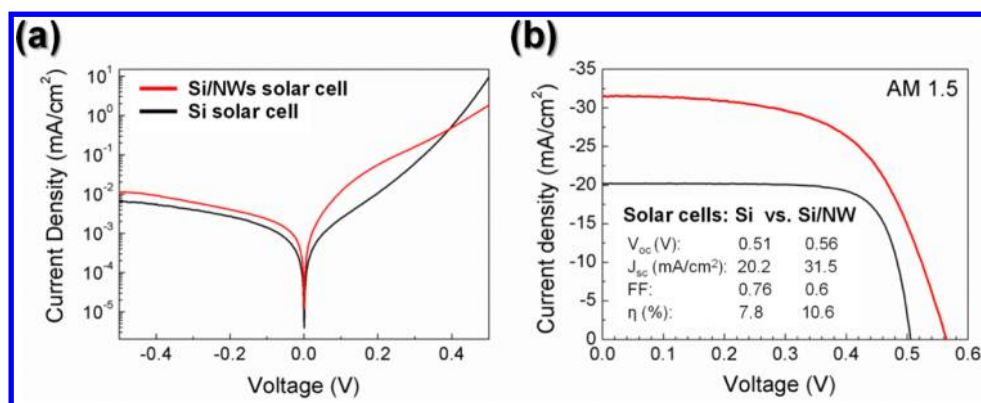
Figure 5. $I-V$ characteristics in (a) dark and (b) under AM 1.5 spectrum illumination for the reference bare Si solar cell (black curve) and Si/NW solar cell (red curve). Semilog and linear scales are used for Y-axis of the graphs in panels a and b, respectively.

passivated by SiO_2 and thus the surface recombination rate is significantly reduced. Similarly, the p^+-NWs here are used as the point-contact and the rest of the Si surface (*i.e.*, more than 98% of area) is passivated with SiN_x. In addition, it was reported that the band alignment of $p-In_{0.53}Ga_{0.47}As$ and p-Si heterojunction is type II, that is, the conduction and valence bands of the $p-In_{0.53}Ga_{0.47}As$ are higher than those of p-Si.[22] If the same band alignment applies to the heavily p-doped $In_{0.7}Ga_{0.3}As$ NW and p-Si heterojunction in our study, it suggests that the shallow barrier at the heterointerface reflects electrons and further reduces the surface recombination rate at the p-Si surface.

Figure 4a shows the external quantum efficiency (EQE) spectra measured from the Si/NW solar cell along with the reference Si solar cell, and Figure 4b plots the normalized EQE. Note that the top surfaces of both Si and Si/NWs solar cells are the same and the rear surface of the bare Si cell has a heavily p^+ doped Si layer (*i.e.*, back-surface-field), instead of the $In_xGa_{1-x}As$ NWs. Remarkably, the EQE of the Si/NW solar cell is higher than that of the reference Si solar cell over almost the entire response wavelength range, with an overall enhancement of 50%. The enhancement in the long wavelength range (>950 nm) can be easily correlated with the increased scattering thus longer optical path length, as shown in Figure 2a. For the short wavelength range, although the absorption efficiency is the same for Si/NW and bare Si, the decrease of total recombination loss through the formation of NW arrays as rear-point-contacts can lead to the enhancement of carrier collection efficiency, thus the increase of photogenerated current.

Shown in Figure 5a is the $I-V$ characteristics of the solar cell devices taken under dark condition. The rectifying ratios of Si solar cells and Si/NWs solar cells are 1.3×10^3 and 1.6×10^2 at ± 0.5 V, respectively, and both devices exhibit a very low reverse leakage current

of $\sim 1 \times 10^{-2}$ mA/cm^2. This confirms that the p^+-type NW array is doped correctly and forms an ohmic contact with the metal layer. Figure 5b shows the $I-V$ characteristics of the solar cells irradiated under the AM 1.5 (100 mW/cm^2) condition at room temperature. The open circuit voltage (V_{oc}), short circuit current (J_{sc}), fill factor (FF), and energy-conversion-efficiency (η) are 0.51 V, 20.2 mA/cm^2, 0.76, and 7.8%, respectively for the reference Si solar cell, and 0.56 V, 31.5 mA/cm^2, 0.6, and 10.6%, respectively for the Si/NWs solar cell. The series resistance calculated from Figure 5b is 1.7 Ω-cm^2 for the Si solar cell, compared to ~ 4 Ω-cm^2 for the Si/NW solar cell. The increase of series resistance for the Si/NW solar cell device could be attributed to the decrease of metal-semiconductor contact area or potential organic residues (*i.e.*, SU8) on the NW tips. In addition, the shunt resistance decrease is also evident from Figure 5b, probably due to nonoptimized process condition. As a result, the FF decreased to 0.6 for the Si/NW solar cell, compared to 0.76 for the reference Si cell. Nevertheless, the V_{oc} and J_{sc} of Si/NW solar cell are higher than those of the reference Si solar cell. The overall energy-conversion-efficiency of the solar cell device shows a 36% increase. This is consistent with the reduction of total recombination loss and increased light absorption resulting from the integration of the $In_xGa_{1-x}As$ NW array.

CONCLUSIONS

In summary, we have reported a new solar cell device structure where $In_xGa_{1-x}As$ NWs are heterogeneously integrated on the back of a Si solar cell. The NW arrays are formed monolithically *via* a catalyst-free self-assembly method. Significant enhancement of EQE and overall energy conversion efficiency has been demonstrated in comparison to the bare Si solar cell. This has been attributed to the reduction of surface recombination loss and increase of light absorption with the NWs acting

as back-reflectors and rear-point-contacts. Further improvement in performance is expected by the optimization of NW structure, composition, and doping.

EXPERIMENTAL PROCEDURES

A MOCVD reactor (Aixtron 200/4) was used for the $In_xGa_{1-x}As$ NW growth. For the solar cell device characterized here, the molar flows of TMIn and TMGa were 1.3×10^{-5} and 7.6×10^{-6} mols/min, respectively. The nominal V/III ratio was 34. Dimethylzinc (DMZn) precursor was used to achieve p^+-type Zn-doped $In_xGa_{1-x}As$ NWs with a molar flow of 7.2×10^{-8} mols/min. The structural properties of $In_xGa_{1-x}As$ NWs were examined using a Hitachi S4800 scanning electron microscope (SEM).

The transmittance spectra of the solar cell devices with the NWs on the back surface (inverted after NWs were grown on the top surface) were obtained using a setup wherein normal incident light illuminated the top planar Si surface, while the transmitted signal was collected from the backside (containing the NWs) of the sample. A GaAs photomultiplier was used for the wavelength range from 0.2 to 0.8 μm and a peltier-cooled PbS detector was used for 0.8 to 2.5 μm. The EQE measurements were obtained using a QEX7 system (PV Measurements, Inc.) A Xe arc emission lamp was coupled to a monochromator with order-sorting filters to select individual wavelengths of light. The light was then chopped, and standard lock-in techniques were used to detect the AC photocurrent at each wavelength. System response was calibrated using a Si photodetector with known responsivity. For each scan, time-dependent variations in lamp intensity were removed using a beam splitter that deflected part of the beam from the monochromator to a known monitor diode, while the rest was diverted to the device under test.

For the solar cell fabrication process, Si substrates were thinned to less than 100 μm using reactive-ion-etching with SF_6 gas chemistry, to maximize the effect of absorption enhancement by the $In_xGa_{1-x}As$ NW array. Next, the samples were thermally annealed with a phosphorus doping source (P_2O_5) at 1000 °C for 10 min to form an n^+ Si contact on the p-type Si wafer. The Si surface with the NWs was covered by a 300 nm SiO_2 layer deposited using plasma-enhanced chemical vapor deposition (PECVD). After thermal annealing, the SiO_2 layer was removed using hydrofluoric acid (HF). Next, a SiN_x layer of 80 nm thickness was then deposited on both sides of the sample, to serve as an ARC as well as a surface passivation layer. Then SU8 was filled in between the NWs and planarized using O_2 plasma RIE until the tips of NWs were exposed. The SiN_x layer on the NW tips was removed using BHF. Finally, Ti/Au (<10/300 nm) metal contacts were formed on the exposed p^+-NW tips. Patterned finger contacts were deposited on the n^+ side. For the reference Si solar cells, a p^+ contact layer was thermally diffused using boron doping sources (B_2O_3) for 20 min at 1000 °C while the n^+ contact layer on the opposite side was protected by SiO_2.

Short circuit current (I_{sc}) and open circuit voltage (V_{oc}) were measured using an AM1.5 solar simulator (100 mW/cm^2). Short circuit current density (J_{sc}) and energy-conversion-efficiency (η) values were calculated using the top planar area of the solar cell, excluding the metal contact area. The total planar dimension of the NW-Si solar cell was ~0.25 cm^2 and the exposed area was 0.1 cm^2.

Conflict of Interest: The authors declare no competing financial interest.

REFERENCES AND NOTES

1. Kayes, B. M.; Atwater, H. A.; Lewis, N. S. Comparison of the Device Physics Principles of Planar and Radial p−n Junction Nanorod Solar Cells. *J. Appl. Phys.* **2005**, *97*, 114302.

2. Kelzenberg, M. D.; Boettcher, S. W.; Petykiewicz, J. A.; Turner-Evans, D. B.; Putnam, M. C.; Warren, E. L.; Spurgeon, J. M.; Briggs, R. M.; Lewis, N. S.; Atwater, H. A. Enhanced Absorption and Carrier Collection in Si Wire Arrays for Photovoltaic Applications. *Nat. Mater.* **2010**, *9*, 239–244.

3. Garnett, E.; Yang, P. Light Trapping in Silicon Nanowire Solar Cells. *Nano Lett.* **2010**, *10*, 1082–1087.

4. Shin, J. C.; Chanda, D.; Chern, W.; Yu, K. J.; Rogers, J. A.; Li, X. Experimental Study of Design Parameters in Silicon Micropillar Array Solar Cells Produced by Soft Lithography and Metal-Assisted Chemical Etching. *IEEE J. Photovoltaics* **2012**, *2*, 129–133.

5. Fang, H.; Li, X.; Song, S.; Xu, Y.; Zhu, J. Fabrication of Slantingly-Aligned Silicon Nanowire Arrays for Solar Cell Applications. *Nanotechnology* **2008**, *19*, 255703.

6. Wolf, S. D.; Agostinelli, G.; Beaucarne, G.; Vitanov, P. Influence of Stoichiometry of Direct Plasma-Enhanced Chemical Vapor Deposited SiN_x Films and Silicon Substrate Surface Roughness on Surface Passivation. *J. Appl. Phys.* **2005**, *97*, 063303.

7. Shin, J. C.; Kim, K. H.; Yu, K. J.; Hu, H.; Yin, L.; Ning, C.-Z.; Rogers, J. A.; Zuo, J.-M.; Li, X. $In_xGa_{1-x}As$ Nanowires on Silicon: One-Dimensional Heterogeneous Epitaxy, Bandgap Engineering, and Photovoltaics. *Nano Lett.* **2011**, *11*, 4831–4838.

8. Noborisaka, J.; Motohisa, J.; Hara, S.; Fukui, T. Fabrication and Characterization of Freestanding GaAs/AlGaAs Core—Shell Nanowires and AlGaAs Nanotubes by Using Selective-Area Metalorganic Vapor Phase Epitaxy. *Appl. Phys. Lett.* **2005**, *87*, 093109.

9. Shin, J. C.; Choi, K. J.; Kim, D. Y.; Choi, W. J.; Li, X. Characteristics of Strain-Induced $In_xGa_{1-x}As$ Nanowires Grown on Si(111) Substrates. *Cryst. Growth Des.* **2012**, *12*, 2994–2998.

10. Chen, C.-C.; Yu, P.; Kuo, H.-C. *Reflectance Study of Nanoscaled Textured Surfaces*. Optical MEMS and Nanophotonics, IEEE/LEOS International Conference on, **2007**, 107−108.

11. Shir, D.; Yoon, J.; Chanda, D.; Ryu, J.-H.; Rogers, J. A. Performance of Ultrathin Silicon Solar Microcells with Nanostructures of Relief Formed by Soft Imprint Lithography for Broad Band Absorption Enhancement. *Nano Lett.* **2010**, *10*, 3041–3046.

12. Dash, W. C.; Newman, R. Intrinsic Optical Absorption in Single-Crystal Germanium and Silicon at 77 K and 300 K. *Phys. Rev.* **1955**, *99*, 1151–1155.

13. Zeng, L.; Bermel, P.; Yi, Y.; Alamariu, B. A.; Broderick, K. A.; Liu, J.; Hong, C.; Duan, X.; Joannopoulos, J.; Kimerling, L. C. Demonstration of Enhanced Absorption in Thin Film Si Solar Cells with Textured Photonic Crystal Back Reflector. *Appl. Phys. Lett.* **2008**, *93*, 221105.

14. Sai, H.; Fujiwara, H.; Kondo, M.; Kanamori, Y. Enhancement of Light Trapping in Thin-Film Hydrogenated Microcrystalline Si Solar Cells Using Back Reflectors with Self-Ordered Dimple Pattern. *Appl. Phys. Lett.* **2008**, *93*, 143501.

15. Biswas, R.; Zhou, D. Simulation and Modelling of Photonic and Plasmonic Crystal Back Reflectors for Efficient Light Trapping. *Phys. stat. sol. (a)* **2010**, *207*, 667–670.

16. McPheeters, C. O.; Yu, E. T. Computational Analysis of Thin Film InGaAs/GaAs Quantum Well Solar Cells with Back Side

Light Trapping Structures. *Opt. Express* **2012**, *20*, A864–A878.

17. Li, X.-H.; Song, R.; Ee, Y.-K.; Kumnorkaew, P.; Gilchrist, J. F.; Tansu, N. Light Extraction Efficiency and Radiation Patterns of III-Nitride Light-Emitting Diodes with Colloidal Microlens Arrays with Various Aspect Ratios. *IEEE Photon. J.* **2011**, *3*, 489–499.

18. Ou, Y.; Jokubavicius, V.; Yakimova, R.; Syväjärvi, M.; Ou, H. Omnidirectional Luminescence Enhancement of Fluorescent SiC *via* Pseudoperiodic Antireflective Subwavelength Structures. *Opt. Lett.* **2012**, *37*, 3816–3818.

19. Koo, W. H.; Youn, W.; Zhu, P.; Li, X.-H.; Tansu, N.; So, F. Light Extraction of Organic Light Emitting Diodes by Defective Hexagonal-Close-Packed Array. *Adv. Funct. Mater.* **2012**, *22*, 3454–3459.

20. Yablonovitch, E.; Cody, G. D. Intensity Enhancement in Textured Optical Sheets for Solar Cells. *IEEE Trans. Electron Devices* **1982**, *29*, 300–305.

21. Zhao, J.; Wang, A.; Green, M. A. 24·5% Efficiency Silicon PERT Cells on MCZ Substrates and 24.7% Efficiency PERL Cells on FZ Substrates. *Prog. Photovolt: Res. Appl.* **1999**, *7*, 471–474.

22. McKay, K. S.; Lu, F. P.; Kim, J.; Yi, C.; Brown, A. S.; Hawkins, A. R. Band Discontinuity Measurements of the Wafer Bonded InGaAs/Si Heterojunction. *Appl. Phys. Lett.* **2007**, *90*, 222111.